

Soft Matter

Accepted Manuscript



This is an *Accepted Manuscript*, which has been through the Royal Society of Chemistry peer review process and has been accepted for publication.

Accepted Manuscripts are published online shortly after acceptance, before technical editing, formatting and proof reading. Using this free service, authors can make their results available to the community, in citable form, before we publish the edited article. We will replace this *Accepted Manuscript* with the edited and formatted *Advance Article* as soon as it is available.

You can find more information about *Accepted Manuscripts* in the [Information for Authors](#).

Please note that technical editing may introduce minor changes to the text and/or graphics, which may alter content. The journal's standard [Terms & Conditions](#) and the [Ethical guidelines](#) still apply. In no event shall the Royal Society of Chemistry be held responsible for any errors or omissions in this *Accepted Manuscript* or any consequences arising from the use of any information it contains.

ARTICLE

Defect Structures and Ordering Behaviours of Diblock Copolymers Self-Assembling on Spherical Substrates

Liangshun Zhang,^{*a} Liquan Wang^a and Jiaping Lin^{*a}

Received 00th January 2012,
Accepted 00th January 2012

DOI: 10.1039/x0xx00000x

www.rsc.org/

One of main differences of ordered structures constrained on curved surfaces is the nature of topological defects. We here explore the defect structures and ordering behaviours of both lamellar and cylindrical phases of block copolymers confined on spherical substrates by the Landau-Brazovskii theory, which is numerically solved by the highly accurate spectral method with a spherical harmonic basis. For the cylindrical phase, the isolated disclinations and scars are generated on the spherical substrates. The number of excess dislocations in a scar depends linearly on the sphere radius. The defect fraction characterizing the ordering dynamics decays exponentially. The scars are formed from the isolated disclinations via the mini-scars. For the lamellar phase, three types of defect structures (hedgehog, spiral and quasi-baseball) are identified. The disclination annihilation is the primary ordering mechanism of lamellar phase.

1 Introduction

As a result of a large number of theoretical and experimental studies, the bulk phase behaviours for linear diblock copolymers have been well mapped out^{1,2}. However, newer technological applications of copolymers for nanolithography, nanosize bioreactors and drug delivery vehicles necessitate tailoring their morphologies^{3,4,5,6}. Confining the block copolymers on substrates introduces geometric frustration to the systems, and allows materials to self-assemble into new nanostructures that are very different from the bulk morphologies. The simple case of block copolymers under confinement is the one-dimensional (1D) confined system, in which the block copolymers are placed between two flat parallel walls. One can observe structures, such as perforated lamellae, parallel or perpendicular lamellae and cylinders^{7,8,9}. The two-dimensional (2D) and three-dimensional (3D) confinements are realized by putting copolymers into cylindrical nanopores and spherical cavities, respectively. A rich and nontrivial variety of nanostructures including helix and toroid are observed or predicted^{10,11,12,13,14,15,16,17}.

One of the main differences of nanostructures of block copolymers confined on the planar (1D) and curved (2D or 3D)

substrates is the nature of topological defects^{18,19}. The curvature of the substrates imposes a topological requirement on the equilibrium structures with defects. For instance, when the lamellar phase of block copolymers is confined on the spherical substrates, requirement of topological constraints should satisfy the Poincaré-Hopf theorem $\sum_i m_i = \chi_E$, where m_i is the charge of i -th defect and $\chi_E=2$ is the Euler characteristic of spherical surfaces. One can deduce the minimum number of defects from the equation. The configurations of lamellar phase confined on the spherical surfaces have at least four $+1/2$ disclination defects or two $+1$ disclination defects. New experimental techniques to create such a 3D confinement are being rapidly developed^{20,21,22,23,24,25,26,27}. Higuchi et al. succeed in preparing various types of complex structures from the diblock copolymers confined in a spherical cavity by a solvent evaporation method²². 3D structural analysis reveals that such $+1/2$ and $+1$ disclination defects are formed in the surface regions of spherical cavity. However, it is much more difficult to experimentally grasp universal principles of defect structures due to the fact that precisely controlling the size and shape of the confining environment is not easily realized by far.

Significant theoretical efforts have been made to understand the defect structures of block copolymers on the flat substrates^{28,29,30}. Nevertheless, theoretical researches regarding the defect structures and ordering kinetics of block copolymers on the curved substrates are very challenging, because they require an accurate representation of substrates and the non-linearity is inherent in the continuum model of this system.

^aShanghai Key Laboratory of Advanced Polymeric Materials, State Key Laboratory of Bioreactor Engineering, Key Laboratory for Ultrafine Materials of Ministry of Education, School of Materials Science and Engineering, East China University of Science and Technology, Shanghai 200237, China. E-mail: zhangls@ecust.edu.cn (L. Zhang); jlin@ecust.edu.cn (J. Lin)

Currently, theoretical and simulation investigations about the defect structures of block copolymers in the curved space are very limited^{31,32,33,34,35,36}. More recently, Chantawansri and co-workers used a self-consistent field (SCF) theory of inhomogeneous polymers to explore microstructures of block copolymers confined on a sphere³³. Three types of defects of lamellar phase are observed for symmetric diblock copolymers. Isolated disclinations are obtained for the cylindrical phase. Nevertheless, the simulations of SCF theory are limited to the cases of small sphere, and cannot capture the defect annihilation of block copolymers confined on the spherical substrates. There remains need for considerable advancements in terms of studying the defect motion of block copolymer nanostructures in the large time scale and thoroughly examining the defect structures.

To address above challenges, we apply the Landau-Brazovskii (LB) theory to study the self-assembly behaviors of block copolymers confined on the spherical substrates. The LB theory of block copolymers can be derived from the many-chain Edwards Hamiltonian following the method of Leibler and Ohta and Kawasaki in the weak segregation limit^{37,38,39}. It has been well established that the LB theory is a convenient way for studying the kinetics of microphase separation of block copolymer systems in the flat space^{40,41,42}. Nevertheless, it has not been implemented in the curved spaces. The primary difficulty in extending the LB theory to the spherical geometry is the numerical solution of non-linear partial differential equations. Here, we develop a spectral collocation algorithm with a spherical harmonic basis, which offers high numerical accuracy and efficiency for solving the equations. The spectral method for the spherical geometry is an extension of the spectral method already used in the fluid dynamics⁴³.

Beyond developing an improved numerical method for solving the LB theory in the curved spaces, we report here on detailed numerical simulations of defect structures and ordering behaviours of both lamellar and cylindrical phases of block copolymers confined on the spherical substrates. This new method is able to produce the defect structures identified by the Delaunay triangulation, and obtain the relationship between the excess dislocations and the sphere radius which, as far as we know, was not predicted by previous simulations on the self-assembly of block copolymers on the spherical surface. The simulations also directly display the defect annihilation, which cannot be observed by the static SCF simulations. Subsequently, we further investigate the defect structures and ordering behaviours of lamellar phase. We expect that the present study may offer a rational understanding about the ordering behaviours of nanostructures on the curved surfaces and some useful information for the design of novel materials of block copolymers.

2 Theoretical model and numerical method

This section introduces the LB theory and our numerical algorithm for solving it. We consider a thin film of AB diblock copolymers confined on the surface of sphere with radius R .

Here, we assume the thickness h of thin film satisfying $h \ll R$. The position- and time-dependent order parameter $\varphi(\mathbf{r}, t) \equiv \varphi_A(\mathbf{r}, t) - f_A$ is the deviation of the A segment density $\varphi_A(\mathbf{r}, t)$ from its average value f_A . The scaled LB free energy functional of such system on the spherical surface S^2 is given by^{41,44}

$$F_{S^2}[\varphi] = \int_{S^2} d\sigma \left\{ \frac{1}{2} [(1 + \nabla_{S^2}^2)\varphi]^2 + \frac{\varepsilon}{2} \varphi^2 - \frac{\varepsilon}{3!} \varphi^3 + \frac{1}{4!} \varphi^4 \right\} \quad (1)$$

where $d\sigma$ is the infinitesimal element of the area and $\nabla_{S^2}^2$ corresponds to the spherical Laplacian operator. The parameter ε is a temperature-like variable, which is related to the Flory-Huggins interaction parameter. The variable s is related to composition asymmetry of copolymers, and vanishes at $f_A = 0.5$. The specific relationships of the above parameters to the composition, polymerization degree and Flory-Huggins interaction parameter are given in References 41 and 45. The phase diagram obtained from the one-mode or two-mode approximation is sketched in Reference 44. Since the order parameter φ is a conserved variable, its dynamics satisfies the following Cahn-Hilliard equation, which is also known as Model B in condensed matter physics⁴⁶

$$\frac{\partial \varphi}{\partial t} = \nabla_{S^2}^2 \frac{\delta F_{S^2}}{\delta \varphi} + \zeta \quad (2)$$

where $\delta F_{S^2} / \delta \varphi$ denotes the functional derivative of free energy functional with respect to φ , and ζ stands for a conserved noise satisfied the fluctuation-dissipation theorem.

Next, the numerical approach to solve the non-linear partial differential equation in the curved space is stated. Rather than using the finite element or finite volume methods, we extend the highly accurate spectral method to solve the Eq. (2). In the flat Euclidian space, an attractive way to solve the non-linear partial differential equations with the periodic boundary conditions is the Fourier spectral method⁴³. Similarly, in the case of the spherical geometry with fixed radius R , the basis of spherical harmonics is chosen, which involves the back and forth transformations between the real- and spectral-space representations. In the real space, the order parameter field $\varphi(\mathbf{r})$ is represented by the spherical-polar coordinate $\mathbf{u}(\phi, \theta)$, where $\phi \in [0, 2\pi)$ denotes the longitude and $\theta \in [-\pi/2, \pi/2]$ denotes the latitude. The spherical harmonic expansion is defined by⁴⁷

$$\varphi(\mathbf{r}) \equiv \varphi(\mathbf{u}) = \sum_{l=0}^{\infty} \sum_{m=-l}^{m=l} \tilde{\varphi}_l^m Y_l^m(\mathbf{u}) \quad (3)$$

where $Y_l^m(\mathbf{u})$ denotes the spherical harmonic of degree l for $-l \leq m \leq l$ and $\tilde{\varphi}_l^m$ are the components of $\varphi(\mathbf{u})$ in the spherical-harmonic space. Since the spherical harmonics are the eigenfunctions of the spherical Laplacian operator, one can calculate the Laplacian of $\varphi(\mathbf{u})$ via application of the operator termwise in the expansion of Eq. (3), which is given by $\nabla_{S^2}^2 \varphi(\mathbf{u}) = \sum_{l=0}^{\infty} \sum_{m=-l}^{m=l} -\frac{l(l+1)}{R^2} \tilde{\varphi}_l^m Y_l^m(\mathbf{u})$. With this, the evolution equation Eq. (2) of order parameter field can be re-expressed in the spherical-harmonic space

$$\frac{\partial \tilde{\varphi}_l^m}{\partial t} = -\frac{l(l+1)}{R^2} \left[\left(\left(1 - \frac{l(l+1)}{R^2} \right)^2 + \varepsilon \right) \tilde{\varphi}_l^m + \tilde{N} L_l^m \right] \quad (4)$$

Here, $\tilde{N} L_l^m$ are the components of nonlinear term $-s \frac{\varphi^2(\mathbf{u})}{2} + \frac{\varphi^3(\mathbf{u})}{3!}$ in the spherical-harmonic space. The conserved noise term of

Eq. (2) is neglected in the spectral method for the sake of numerical simplification. The above equations for the order parameter field φ_l^m are numerically solved by a semi-implicit scheme in the equally space grid⁴⁸. The back and forth transformations between the real space and spherical-harmonic space are performed by using the SPHEREPACK 3.2 software package⁴⁹.

In our simulations, the initial configurations are the disordered states, in which uniform random numbers between -0.1 and 0.1 are assigned to the order parameter field at the lattice sites of spherical surface. To ensure that the observed defect structures are not accidental, we repeat the simulations for 10 times using different initial random configurations. Usually, the initial configurations quickly evolve into the ordered structures. However, for a quenching system with large sphere radius, the configurations still contain lots of defects even after a long-time run due to a kinetically slow process of defect annihilation. To promote the escape of metastable configurations, an annealing process is subsequently performed. Specifically, the initial configurations of annealing process are the final states of quenching simulations. The parameter ε is linearly increased with the simulation step, but kept below the critical value of disorder-to-order transition, and then linearly decreased to the initial setting value ε_0 . The above procedure is cycled 6~10 times until the total energy of system with ε_0 at different cycles does not change. The annealing process used in our simulations may correspond to the multi-cycle annealing process in the experiments, which has been applied to prepare highly-aligned patterns of block copolymers in the Harrison et al. study²⁸.

3 Results and discussion

In contrast to the microphase separation of block copolymers in the flat space, the nanostructures of block copolymers confined on the spherical substrates depend not only on the parameters ε_0 and s , but also on the curvature of sphere. The topology of the sphere enforces a requirement of defect structures in the equilibrium configurations. In what following, we investigate the defects and ordering processes of both cylindrical and lamellar phases of diblock copolymers confined on the surfaces of spheres with different radii.

3.1 Defect structures and ordering behaviours of cylindrical phase

In this subsection, we choose the parameters $\varepsilon_0 = -0.13$ and $s = 0.3$, which correspond to the case of asymmetric block copolymers. The cylindrical phase is stability⁴⁴. In order to determine the defect structures of cylindrical phase on the spherical surfaces, two main steps are performed during the standard data post-processing. In the first step, the cores or vertexes of cylinder domains are determined through the local maxima of order parameter field. In the second step, the algorithm of Delaunay triangulation with these vertexes in the curved space is conducted⁵⁰. It is useful to visualize the defect structures through diagrams shown in Figures 1(b) and 2(b), which are

constructed by lines connecting a vertex (represented by a small sphere) with all of its neighbours. The number of lines of a vertex is used to identify the defect types. The five-fold and seven-fold coordinated vertexes can be respectively characterized by the disclination charges +1 and -1, which are the departure of the coordination number from the flat space value of 6. A tightly bound pair of +1 and -1 disclinations forms a dislocation.

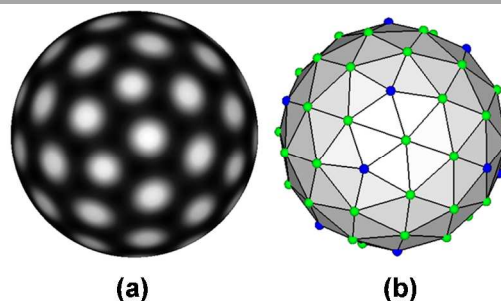


Fig. 1 (a) Profile of order parameter field for 60 cylinder domains on the surface of a sphere with radius $R \approx 2.0a$ (a is the mean distance of cylinder pairs). White and gray colors refer to large and small values of order parameter field, respectively. (b) Associated diagram of Delaunay triangulation for the cylinders or vertexes on the spherical surface. The vertexes symbolised by the small spheres denote the centres of cylinder domains. Five-fold, six-fold and seven-fold coordinated vertexes are colored by blue, green and red, respectively. The solid lines represent the connections of a vertex with its neighbours.

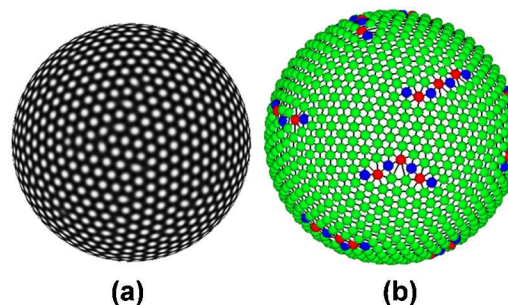


Fig. 2 (a) Profile of order parameter field for 1052 cylinder domains on the surface of a sphere with radius $R \approx 8.20a$. (b) Associated diagram of Delaunay triangulation for the cylinders or vertexes on the spherical surface. The representations of colors, symbols and lines are the same as Figure 1. The small spheres with red color denote the vertexes with seven-fold coordinated sites.

DEFECT STRUCTURES OF CYLINDRICAL PHASE Figure 1(a) shows the profile of order parameter field on the surface of a sphere with radius $R \approx 2.0a$, where a is the average distance of the cylinder pairs. The order parameter field on the closed surface is represented as a gray-white field, where the gray and white colors correspond to the small and large values of order parameter field, respectively. This configuration contains 60 cylinders arranged on the spherical substrate. The associated diagram of Delaunay triangulation is illustrated in Figure 1(b). The vertexes correspond to the local maxima of order parameter. 12 isolated +1 disclinations (five-fold coordinated sites) are observed in the Delaunay diagram. In the flat space, the isolated +1 disclinations are not usually found because they produce large distortions in the configuration. On the contrary, on the curved substrates, the disclinations help to screen out the geometric frustration to reduce the distortions¹⁹. In the multi-cycle annealing process, the isolated +1 disclinations cannot be

removed away. This phenomenon manifests the fact that the isolated +1 disclinations are an intrinsic part of the configurations on the spherical substrates.

As the total number of cylinder domains or sphere radius increases, the dislocations are introduced into the system to further reduce the distortions of isolated +1 disclinations. For instance, the system with sphere radius $R \approx 8.20a$ is quenched from the random initial configuration, and the annealing process is subsequently performed. As shown in Figure 2(a), the cylinders are arranged on the spherical surface, and the final configuration of order parameter field consists of 1052 cylinders. Figure 2(b) is the associated diagram of Delaunay triangulation, which contains 51 five-fold, 962 six-fold and 39 seven-fold coordinated sites. The isolated +1 or -1 disclinations are not observed in the final configuration. One can observe that pairs of +1 and -1 disclinations produce chains of dislocations. Note that a chain of 5-7 pair dislocations arranged around an unpaired +1 disclination, *i.e.*, 5-7-5-7-5-7-5, is illustrated in Figure 2(b). The defect structures are called scars, which are experimentally observed in the spherical crystals⁵¹. Here, the number of excess dislocations in a scar has a value of 3. It should be mentioned that the scars cannot be further annihilated in the annealing simulations, suggesting that the scar structures are an intrinsic part of configurations on the spherical surfaces.

To quantify the behaviours of the scars, we determine the mean number of excess dislocations in a scar from the diagram of Delaunay triangulation, and plot the result as a function of the relative sphere radius R/a , which is displayed in Figure 3. Each data point is collected from ten independent runs. Below the critical value of the relative sphere radius $(R/a)_c \approx 5.0$, only 12 isolated +1 disclinations are observed, and the dislocations cannot be produced in this system. As the sphere radius increases, the isolated disclinations become much more energetically cost, while the formation of dislocation chains may reduce the energy. Above the critical value of $(R/a)_c$, the mean number of excess dislocations in a scar increases with the relative sphere radius. In the range of large sphere radius, the number of excess dislocations in a scar grows proportional to the relative sphere radius, and the obtained best-fit slope is 0.435. Since the different initial states result in the metastable configurations with different amount of excess dislocations in a scar, non-integer number of dislocation appears in Figure 3 due to the averaging of several runs.

ORDERING BEHAVIOURS OF CYLINDRICAL PHASE Upon quenching the system below the critical value of disorder-to-order transition, the initial configurations with small random fluctuations evolve into the ordered patterns. To characterize order degree of cylinder nanostructures, we calculate defect fraction to monitor the ordering dynamics. The defect fraction at time t is defined as $DF(t) = (N - V_6) / N \times 100\%$ ^{52,53}, where V_6 and N are the number of six-fold coordinated vertexes and the total number of vertexes in the diagram of Delaunay triangulation, respectively. Here, we do not distinguish the defects with five-fold (+1), seven-fold (-1), or other coordinated sites, and only the total defects are collected from the diagram of Delaunay

triangulation. The typical temporal evolution of the defect fraction is shown in Figure 4. From the double-logarithmic plot, one can see that there are two stages in the ordering process of cylindrical phase on the spherical surfaces. The defect fraction as a function of time t obeys a power law $DF(t) \propto t^{-1/3}$ for the time from 0 to $10^2\tau$, and $DF(t) \propto t^{-1/5}$ for the time from $10^2\tau$ to $10^3\tau$. Here, τ is the time unit in simulations. At the early stage of ordering process, the spherical substrate cannot affect the kinetic behaviour, which obeys the evaporation-condensation mechanism derived by Lifshitz and Slyozov in the flat space⁵⁴. As time proceeds, the decay of defect fraction is slower than that of early stage, and the defect annihilation is strongly affected by the geometrical characteristics of the substrates. It should be mentioned that the sphere radius can affect the transition time of scaling law in the quenching simulations.

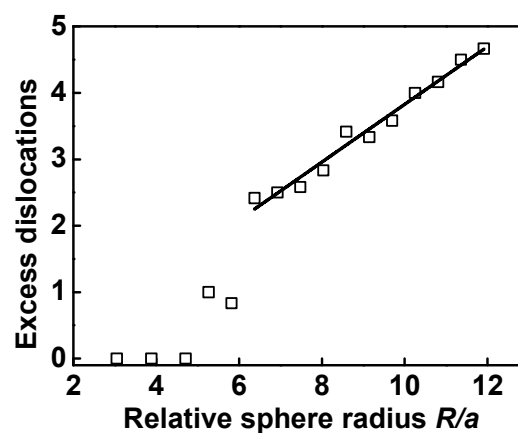


Fig. 3 Mean number of excess dislocations in a scar as a function of relative sphere radius R/a . All the data points represent the average value of ten samples. The solid line is the best-fit curve in the range of large spherical radius, and the obtained slope is 0.435.

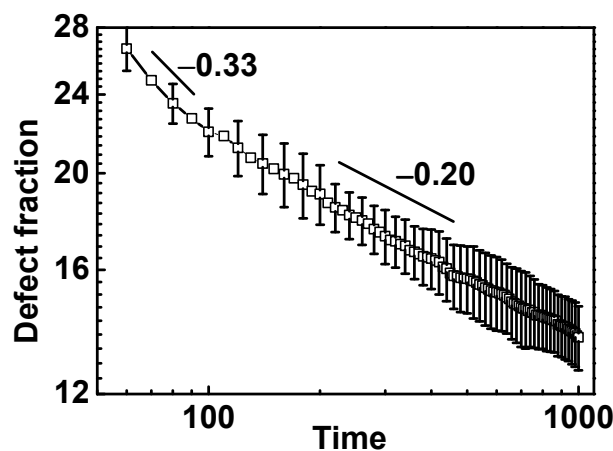


Fig. 4 Typical time evolution of defect fraction of cylindrical phase on the spherical surface during the quenching simulation. The defect fraction at time t is defined as $DF(t) = (N - V_6) / N \times 100\%$, where V_6 and N are the number of six-fold coordinated vertexes and the total number of vertexes in the diagram of Delaunay triangulation, respectively. Each data point is collected from ten independent runs. The error bars are successively skipped one point for the sake of clarity. Two solid lines represent the best-fit power laws in the ranges of early and intermediate stages of ordering process.

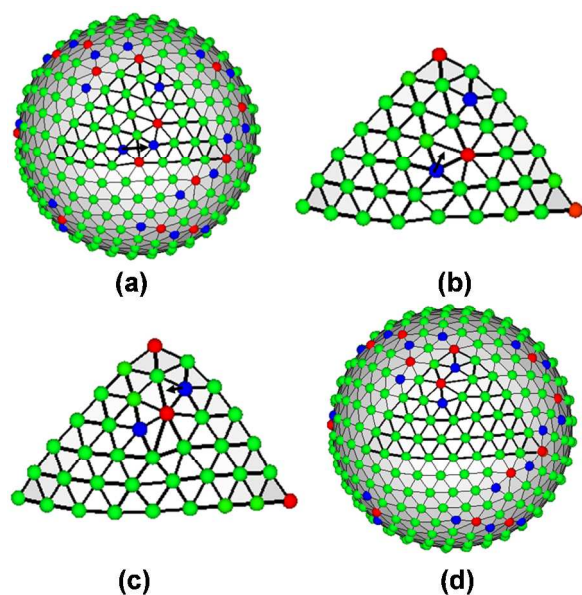


Fig. 5 Typical formation process of a scar within the highlight area. Time: (a) $\Delta t/\tau=0$, (b) $\Delta t/\tau=35$, (c) $\Delta t/\tau=90$, and (d) $\Delta t/\tau=155$. Here, τ is time unit in simulations. Snapshot (a) displays the initial configuration from the quenching simulation, while snapshot (d) displays the configuration where a scar is formed within the highlight area. For the sake of clarity, only one portion of diagram of Delaunay triangulation is drawn in snapshots (b) and (c). The representations of colors, symbols and lines are the same as Figure 1. The arrows indicate the motion directions of vertices.

At the late stage of simulations, the total number of cylinder domains does not further change, but the scars are generated by the local motion of disclinations and dislocations. Figure 5 shows the formation of a scar on the spherical surface at the late stage of quenching simulation. Snapshots (a) and (d) are the initial and final configurations of scar formation within the highlight area, respectively. For the sake of clarity, snapshots (b) and (c) display a portion of configurations. In the bottom of highlight area, there is a high-angle grain boundary, as shown in Figure 5(a). The near $+1$ disclinations are unstable, and start to locally re-arrange. A new 5-7 pair dislocation is generated (Figure 5(b)). Subsequently, the new dislocation glides towards the nearest isolated $+1$ disclination, and quickly forms a mini-scar (5-7-5 grain boundary), which is illustrated in Figure 5(c). Eventually, the mini-scar further joins the nearest 5-7 pair dislocation to generate a 5-7-5-7-5 scar (Figure 5(d)).

The formation of scars on the spherical surfaces is similar to the experimental and theoretical works of Bowick et al.^{55,56} In their works, one colloid is added to or subtracted from initial structures of spherical crystals. The curvature of sphere drives formation of dislocations. The individual dislocation then glides towards the nearest isolated disclination. The dislocation binding with the disclination forms 5-7-5 mini-scar. As shown in Figures 5(b) to 5(d), the formation of scars from isolated $+1$ disclinations via mini-scars is observed. The process of scar formation is in generally agreement with the findings of Bowick et al.

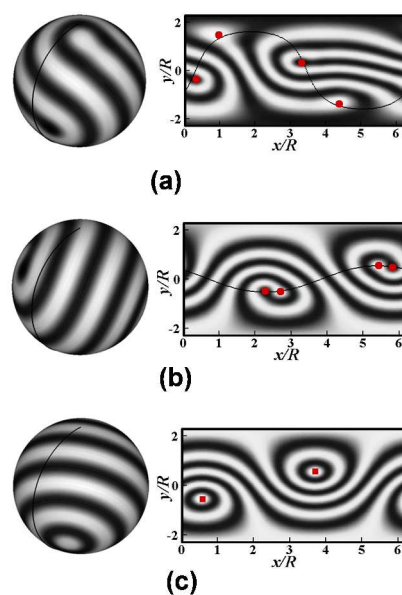


Fig. 6 Defect structures of lamellar phase confined on the spherical substrates. (a) System size $2\pi R/d \approx 10.0$, quasi-baseball defect structure; (b) System size $2\pi R/d \approx 11.0$, spiral defect structure; and (c) System size $2\pi R/d \approx 12.0$, hedgehog defect structure. White (gray) color refers to large (small) value of order parameter field. Left column is the profiles of order parameter field on the spherical surfaces. The curve on the spherical surface denotes the longitude $\phi = 0$ and the range of latitude $\theta \in [-\pi/2, \pi/2]$. Right column is the modified Mercator projections of the order parameter field. The horizontal and vertical axes respectively refer to the $x = R\phi$ and $y = \frac{2}{\pi}R \ln(\tan(\frac{\pi}{4} + \frac{\theta}{2}))$, where $\phi \in [0, 2\pi)$ denotes the longitude and $\theta \in [-\pi/2, \pi/2]$ denotes the latitude. The red circles and squares represent the cores of $+1/2$ and $+1$ disclinations, respectively. The curve in the projection represents a great circle passed through the defect cores.

We wish to emphasize that, although the LB theory of block copolymers can predict the scar structures and scar formation, there exists a significant difference between the block copolymers and colloids confined on the spherical surfaces. In system of colloids, the shape and size of colloids are not perturbed by the strain field of defects, and the number of colloids is fixed in the particle motion. However, the polymer chains can stretch to change the shape of the cylinder domains due to the strain field introduced by the disclinations, and the coalescence of cylinder domains may take place in the evolution. These result in the fact that the number of cylinder domains is not a conserved variable. Therefore, for the system of colloids, the kinetic behaviors of defect structures may experience some degree of variations.

3.2 Defect structures and ordering behaviours of lamellar phase

In this subsection, we turn to investigate the lamellar phase of symmetric block copolymers confined on the spherical substrates. The parameters are set as $\varepsilon_0 = -0.2$ and $s = 0$.⁴⁴ The system size is characterized by the ratio $2\pi R/d$, where R is the sphere radius and d is the averaging repeat spacing of lamellae. In the present work, because of the difficulty in the automated recognition algorithm of defect structures of lamellar configuration in the curved space, we only concentrate on the defect structures and ordering process of lamellar phase on the spherical surfaces.

DEFECT STRUCTURES OF LAMELLAR PHASE The lamellar phase is analogous to the smectic-A liquid crystals. Here, we use the type of defects of liquid crystals to characterize the defect structures of lamellar phase. The $+1/2$ and $+1$ disclinations are illustrated in Figure 6. More details about the defects of liquid crystals can be found in the monograph of de Gennes and Prost⁵⁷.

Figure 6 summarizes the obtained defect structures of lamellar phase on the surface of a sphere with small radius in the multi-cycle annealing simulations. Left column in Figure 6 displays the profiles of order parameter field on the spherical surfaces. To gain a better view of the corresponding configuration on the spherical surface, we also plot the modified Mercator projections, which are illustrated in the right column of Figure 6. The horizontal and vertical axes respectively refer to the $x = R\phi$ and $y = \frac{5}{4}R \ln(\tan(\frac{\pi}{4} + \frac{2}{5}\theta))$, where $\phi \in [0, 2\pi)$ denotes the longitude and $\theta \in [-\pi/2, \pi/2]$ denotes the latitude. Here, the defect structures of lamellar phase on the spherical substrates could be empirically classified into three categories³³. The first class is the quasi-baseball defect structure, as shown in Figure 6(a). Four $+1/2$ disclinations denoted by the red circle symbols are equally spaced at 90° intervals on a great circle. The quasi-baseball structure contains more than two stripes. The strip termination can appear at the core of each disclinations. The second class, as illustrated in Figure 6(b), is called the spiral defect structure. The structure has the same number of disclinations as the quasi-baseball structure. However, the four $+1/2$ disclinations are not evenly spaced. The spiral structure contains only two continuous stripes. The stripes are spirals around the cores of disclinations, and terminate at the centre of other disclinations. The third class is called the hedgehog defect structure, as observed in Figure 6(c). All stripes are circularly arranged on the spherical surface, and there are two $+1$ disclinations at the two opposite positions of the sphere. It should be noted that Chantawansri et al. developed a self-consistent field theory in the spherical geometry to investigate the defect structures of lamellar phase of block copolymers³³. The defect structures including hedgehog, quasi-baseball and spiral are predicted in their calculations. Furthermore, by quantitatively analysing the free energy density of the structures, they found that the quasi-baseball defect structure is metastable, and its energy is close to that of spiral defect structure.

It is difficult at this time to make a comprehensive comparison between the theoretical predictions and experimental observations due to limited experimental studies on self-assembly behaviours of block copolymers confined on the spherical substrates. However, we can still compare the calculation results with some existing studies. For example, Higuchi et al. reported microphase-separated structures of polystyrene-*block*-polyisoprene (PS-*b*-PI) by 3D confinement²². A 3D reconstructed technique is used to identify the nanostructures of block copolymers. They found that the complex structures are only formed in the surface region of sphere cavity. Ring structures of PS phase and PI phase are arranged at the spherical surface. Another type of morphologies

is the “helix” structures, where the PS phase twists around the PI phase. According to the simulation results, when the symmetric block copolymers are confined on the spherical surfaces, the lamellae are circularly arranged on the spherical surface (Figure 6(c)), which corresponds to the ring structure in experiment. As shown in Figure 6(b), two continuous lamellae mutually twist. This structure is very similar to the “helix” structure in experiment.

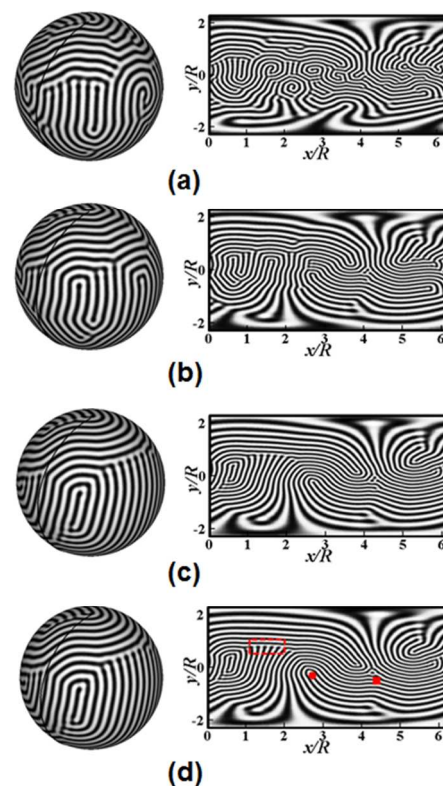


Fig. 7 Snapshots of ordering process of lamellar phase in the quenching simulation. Time: (a) $t/\tau=300$, (b) $t/\tau=5000$, (c) $t/\tau=28000$, and (d) $t/\tau=50000$. Left column is the profiles of order parameter field on the surface of a sphere with $2\pi R/d \approx 51.0$. Right column is the modified Mercator projections of the order parameter field. The representations are the same as Figure 6. In panel (d), the red circle and square denote respectively the cores of disclination and dislocation, and the dashed box encloses the grain boundary.

ORDERING BEHAVIOURS OF LAMELLAR PHASE Figure 7 shows the evolution of lamellar phase confined on the surface of a sphere with large radius after a quenching from the homogenous state. Due to the disordered initial configuration, randomly distributed lamellae are observed at the early time (Figure 7(a)). The poorly oriented lamellae locally re-arrange to form the highly-aligned lamellae, and the dislocations and multi-poles of disclinations are annihilated by the motion of defects. The facts result in an increase of order degree of lamellar configuration at the intermediate stage (Figures 7(b) and 7(c)). In the quenching simulation of system with large sphere radius, the resulting configuration is usually “polycrystalline” state with randomly oriented lamellae. Figure 7(d) illustrates the final configuration of lamellae on the surface of a sphere with radius $2\pi R/d \approx 51.0$. The characteristic of such

configuration is the presence of large amount of defects, such as grain boundaries, dislocations and disclinations, which are also highlighted in Figure 7(d). Comparison between the configurations of different times $t=2.8\times 10^4\tau$ (Figures 7(c)) and $t=5.0\times 10^4\tau$ (Figure 7(d)) indicates that the evolution of order parameter field cannot further annihilate the defects, and the configuration remains practically constant beyond $t=5.0\times 10^4\tau$ in the quenching simulation.

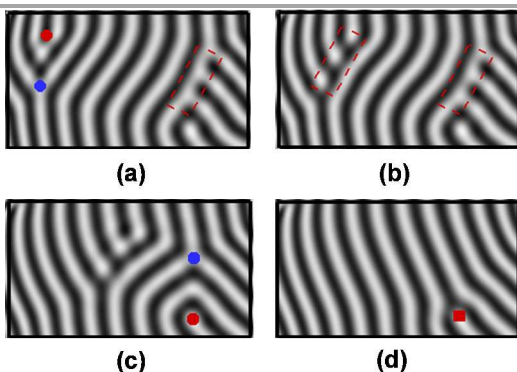


Fig. 8 Snapshots of defect annihilation. (a) $\Delta t/\tau=0$, the spacing between the disclination dipole and the grain boundary is widely separated. (b) $\Delta t/\tau=4600$, the dipole of disclinations evolves into a grain boundary. (c) $\Delta t/\tau=5900$, the spacing between the defects decreases. (d) $\Delta t/\tau=6200$, the number of defects is decreased, but a dislocation still exists in the bottom right. The panels are only a portion of the lamellar phase on the spherical surface. The cores of $+1/2$ disclinations, $-1/2$ disclinations and dislocation are indicated by the red circles, blue circles and red square, respectively. The grain boundaries are enclosed by the dashed boxes.

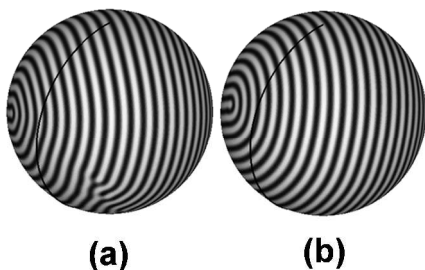


Fig. 9 Snapshots of ordering process in the annealing process. The initial state is the configuration of Figure 7(d). (a) Configuration after 6 cycles of annealing process and (b) configuration after 10 cycles of annealing process.

A typical example of defect annihilation on the spherical substrate is illustrated in Figure 8. A portion of the lamellar configuration is extracted from the profile of order parameter field on the spherical surface. Panel (a) shows a disclination dipole with the $+1/2$ and $-1/2$ disclination cores, and a grain boundary evolving from a disclination dipole. The spacing between them is widely separated. The high strain energy of the disclination dipole causes the defects to evolve. The fact gives rise to production of a grain boundary, as observed in the left of panel (b). Subsequently, this defect structure climbs normal to the boundary, and the defect motion reduces the separation distance of defect pairs, which is illustrated in panel (c). The disclination dipole in the bottom right of panel (c) is the result of defect motion, which is out of the portion of the lamellar configuration. Finally in panel (d), the disclination dipole and grain boundary are annihilated by the local motion of defects to

reduce the strain energy, and only a dislocation remains in the panel.

The type of defect annihilation described above is the main mechanism of ordering process of lamellar phase on the spherical surfaces for the set of parameters chosen in this study. It is very similar to the defect annihilation identified by Harrison et al. on the flat substrates. Harrison et al. studied the ordering dynamics of the lamellar phase of block copolymers in a thin film²⁸. The results reveal that the annihilation of quadrupole consisting of two disclination pairs is the dominant mechanism of ordering process. Like the Harrison's study, the process of defect annihilation in our simulations involves the disclinations and grain boundaries. As shown in Figure 8, the grain boundary evolves from the disclination dipole, and reorganizes into a disclination dipole due to the defect motion. Thus, the ordering mechanism in our simulations is very similar to the experimental findings by Harrison et al. It should be mentioned that the annihilation of dislocations is not frequently observed due to the small size of system in our simulations.

Unlike the intrinsic defects on the spherical surfaces (Figure 6), the defects of lamellar phase on the surface of a large sphere can be further annihilated by the annealing simulation. Figure 9 shows the ordering process of lamellar phase in the subsequent annealing process. The initial state is the configuration with defects of grain boundaries, dislocations and disclinations (Figure 7(d)). After several cycles of annealing process, the defects of lamellar configuration are gradually annihilated, and the lamellar patterns with highly-aligned order on the spherical surface are observed in Figure 9(a). After sufficient cycles of annealing process, the well-aligned lamellae dominate the spherical surface (Figure 9(b)). However, the four $+1/2$ disclinations located on a great circle still exist on the spherical surface. The nearest cores of disclinations are separated by about 4 stripes. According to the classification of defects, the defect structure of this lamellar configuration is spiral.

Although the LB model and spectral method presented here provide a powerful methodology for studying the defect structures and ordering behaviours of block copolymers on the spherical substrates, there are still some drawbacks for the cases of tackling the complex systems or geometries. Here, a few comments on the model and numerical method are in order. First of all, for the complex systems containing the block copolymers, there are certainly some opportunities to improve the model. For instance, the free energy functional used in the model is a simplification form of density functional theories in the weak segregation limit, and does not explicitly take into account the conformational entropy of polymer chains. To solve this problem, one can replace Eq. (1) with a free energy form of coarse-grained microscopic model, *e.g.*, self-consistent mean-field theory of inhomogeneous polymers, which accounts for the chain connectivity and provides a unified treatment of polymer systems from the weak to strong segregation regions⁵⁸. With these improvements, one can accurately calculate the free energy of different structures, and distinguish the metastable configurations of spiral and quasi-baseball defects on the spherical substrates.

Secondly, the surface topology in our present study is the spherical geometry, and a spherical harmonic basis is adopted to numerically solve the model equations. It is difficult to extend the numerical method used in our simulations to more complex geometries ranging from ellipsoids to cylinders and spheres with a bump. To overcome the drawback, Marenduzzo et al. recently proposed a modified finite element algorithm to discretize the Laplace-Beltrami operator and non-linear terms of free energy⁵⁹. They applied the algorithm to tackle the problems of phase separation dynamics on the non-spherical surfaces. It is possible to extend the finite element scheme to solve the equations of LB model or self-consistent field theory of polymers, and to investigate the defect structures and dynamics behaviours of block copolymers on the complex geometries, such as the negative-curvature surfaces.

4 Conclusions

In summary, the LB model of block copolymers, which is numerically solved by the spectral method with a spherical harmonic basis, is used to investigate the defect structures and ordering dynamics of both cylindrical and lamellar phases on the spherical substrates. For the cylindrical phase, the isolated disclinations emerge in the system with small sphere radius. The scars are formed on the surface of a sphere with large radius, and the number of excess dislocations in a scar is linearly proportional to the sphere radius. The defect fraction of cylindrical phase exponentially decays, and the formation of scars from isolated disclinations via mini-scars was observed. For the lamellar phase, the defect structures of the hedgehog, spiral and quasi-baseball are produced on the spherical substrates, and the disclination annihilation is the dominant ordering mechanism of lamellar phase.

Acknowledgments

This work was supported by the National Natural Science Foundation of China (51203049, 21234002), and Research Fund for the Doctoral Program of Higher Education of China (20120074120003).

Notes and references

- 1 M. W. Matsen and M. Schick, *Phys. Rev. Lett.*, 1994, **72**, 2660.
- 2 E. W. Cochran, C. J. Garcia-Cervera and G. H. Fredrickson, *Macromolecules*, 2006, **39**, 2449.
- 3 M. Park, C. Harrison, P. M. Chaikin, R. A. Register and D. H. Adamson, *Science*, 1997, **276**, 1401.
- 4 A. M. Jackson, J. W. Myerson and F. Stellacci, *Nat. Mater.*, 2004, **3**, 330.
- 5 C. Park, J. Yoon and E. L. Thomas, *Polymer*, 2003, **44**, 6725.
- 6 P. Broz, S. Driamov, J. Ziegler, N. Ben-Haim, S. Marsch, W. Meier and P. Hunziker, *Nano Lett.*, 2006, **6**, 2349.
- 7 H. P. Huinink, M. A. van Dijk, J. C. M. Brokken-Zijp and G. J. A. Sevink, *Macromolecules*, 2001, **34**, 5325.

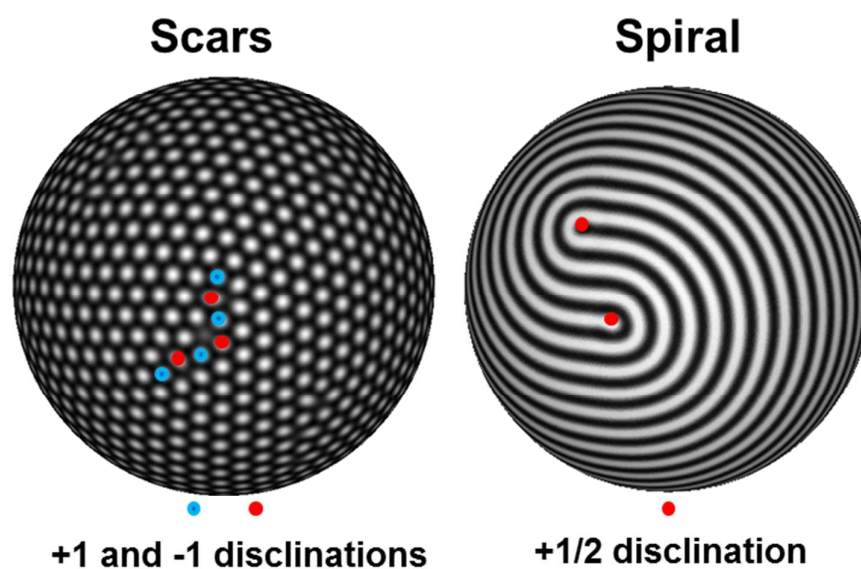
- 8 Q. Wang, P. F. Nealey and J. J. de Pablo, *Macromolecules*, 2001, **34**, 3458.
- 9 A. Knoll, A. Horvat, K. S. Lyakhova, G. Krausch, G. J. A. Sevink, A. V. Zvelindovsky and R. Magerle, *Phys. Rev. Lett.*, 2002, **89**, 035501.
- 10 Y. Wu, G. Cheng, K. Katsov, S. W. Sides, J. Wang, J. Tang, G. H. Fredrickson, M. Moskovits and G. D. Stucky, *Nat. Mater.*, 2004, **3**, 816.
- 11 H. Xiang, K. Shin, T. Kim, S. Moon, T. J. McCarthy and T. P. Russell, *J. Polym. Sci., Part B: Polym. Phys.*, 2005, **43**, 3377.
- 12 W. Li, R. A. Wickham and R. A. Garbary, *Macromolecules*, 2006, **39**, 806.
- 13 P. Chen, X. He and H. Liang, *J. Chem. Phys.*, 2006, **124**, 104906.
- 14 B. Yu, P. Sun, T. Chen, Q. Jin, D. Ding, B. Li and A.-C. Shi, *Phys. Rev. Lett.*, 2006, **96**, 138306.
- 15 J. G. E. M. Fraaije and G. J. A. Sevink, *Macromolecules*, 2003, **36**, 7891.
- 16 B. Yu, B. Li, Q. Jin, D. Ding and A.-C. Shi, *Soft Matter*, 2011, **7**, 10227.
- 17 C. R. Stewart-Sloan and E. L. Thomas, *Eur. Polym. J.*, 2011, **47**, 630.
- 18 D. R. Nelson, *Nano Lett.*, 2002, **2**, 1125.
- 19 P. Chaikin and T. Lubensky, *Principles of Condensed Matter Physics*, Cambridge University Press, 1995.
- 20 H. Yabu, T. Higuchi and M. Shimomura, *Adv. Mater.*, 2005, **17**, 2062.
- 21 T. Higuchi, A. Tajima, K. Motoyoshi, H. Yabu and M. Shimomura, *Angew. Chem. Int. Ed.*, 2008, **47**, 8044.
- 22 T. Higuchi, K. Motoyoshi, H. Sugimori, H. Jinnai, H. Yabu and M. Shimomura, *Soft Matter*, 2012, **8**, 3791.
- 23 N. Saito, R. Takekoh, R. Nakatsuru and M. Okubo, *Langmuir*, 2007, **23**, 5978.
- 24 S. J. Jeon, G. R. Yi, C. M. Koo and S. M. Yang, *Macromolecules*, 2007, **40**, 8430.
- 25 S. J. Jeon, G. R. Yi and S. M. Yang, *Adv. Mater.*, 2008, **20**, 4103.
- 26 D. A. Rider, J. I. L. Chen, J.-C. Eloi, A. C. Arsenault, T. P. Russell, G. A. Ozin and I. Manners, *Macromolecules*, 2008, **41**, 2250.
- 27 S. G. Jang, D. J. Audus, D. Klinger, D. V. Krogstad, B. J. Kim, A. Cameron, S.-W. Kim, K. T. Delaney, S.-M. Hur, K. L. Killops, G. H. Fredrickson, E. J. Kramer and C. J. Hawker, *J. Am. Chem. Soc.*, 2013, **135**, 6649.
- 28 C. Harrison, H. Adamson, Z. Cheng, J. M. Sebastian, S. Sethuraman, D. A. Huse, R. A. Register and P. M. Chaikin, *Science*, 2000, **290**, 1558.
- 29 D. A. Vega, C. K. Harrison, D. E. Angelescu, M. L. Trawick, D. A. Huse, P. M. Chaikin and R. A. Register, *Phys. Rev. E*, 2005, **71**, 061803.
- 30 R. A. Segalman, A. Hexemer, R. C. Hayward and E. J. Kramer, *Macromolecules*, 2003, **36**, 3272.
- 31 P. Tang, F. Qiu, H. Zhang and Y. Yang, *Phys. Rev. E*, 2005, **72**, 016710.
- 32 J. F. Li, J. Fan, H. D. Zhang, F. Qiu, P. Tang and Y. Yang, *Eur. Phys. J. E*, 2006, **20**, 449.

- 33 T. L. Chantawansri, A. W. Bosse, A. Hexemer, H. D. Ceniceros, C. J. Garcia-Cervera, E. J. Kramer and G. H. Fredrickson, *Phys. Rev. E*, 2007, **75**, 031802.
- 34 B. Vorselaars, J. U. Kim, T. L. Chantawansri, G. H. Fredrickson and M. W. Matsen, *Soft Matter*, 2011, **7**, 5128.
- 35 L. R. Gómez and D. A. Vega, *Phys. Rev. E*, 2009, **79**, 031701.
- 36 M. Pinna, S. Hittl, X. Guo, A. Böker and A. V. Zvelindosky, *ACS Nano*, 2010, **4**, 2845.
- 37 S. A. Brazovskii, *Sov. Phys. JETP*, 1975, **41**, 85.
- 38 L. Leibler, *Macromolecules*, 1980, **13**, 1602.
- 39 T. Ohta and K. Kawasaki, *Macromolecules*, 1986, **19**, 2621.
- 40 S. Qi and Z.-G. Wang, *Phys. Rev. Lett.*, 1996, **76**, 1679.
- 41 R. A. Wickham and A.-C. Shi, *J. Chem. Phys.*, 2003, **118**, 10293.
- 42 M. Pinna and A. V. Zvelindovsky, *Eur. Phys. J. B*, 2012, **85**, 210.
- 43 C. Canuto, M. Y. Hussaini, A. Quarteroni and T. A. Zang, *Spectral Methods in Fluid Dynamics*, Springer, 1988.
- 44 I. W. Hamley and V. E. Podneks, *Macromolecules*, 1997, **30**, 3701.
- 45 G. H. Fredrickson and E. Helfand, *J. Chem. Phys.*, 1987, **87**, 697.
- 46 P. C. Hohenberg and B. I. Halperin, *Rev. Modern Phys.*, 1977, **49**, 435.
- 47 G. B. Arfken and H. J. Weber, *Mathematical Methods for Physicists, 6th ed.: A Comprehensive Guide*, Academic Press, 2005
- 48 W. Press, S. Teukolsky, W. Vetterling and B. Flannery, *Numerical Recipes in Fortran: the Art of Scientific Computing*, Cornell University Press, 1992.
- 49 J. C. Adams and P. N. Swarztrauber, *Mon. Weather Rev.*, 1999, **127**, 1872.
- 50 R. J. Renka, *ACM Trans. Math. Softw.*, 1997, **23**, 416.
- 51 R. Bausch, M. J. Bowick, A. Cacciuto, A. D. Dinsmore, M. F. Hsu, D. R. Nelson, M. G. Nikolaides, A. Travasset and D. A. Weitz, *Science*, 2003, **299**, 1716.
- 52 Y. Yokojima and Y. Shiwa, *Phys. Rev. E*, 2002, **65**, 056308.
- 53 H. Qian and G. F. Mazenko, *Phys. Rev. E*, 2003, **67**, 036102.
- 54 M. Lifshitz and V. V. Slyozov, *J. Phys. Chem. Solids*, 1961, **19**, 35.
- 55 P. Lipowsky, M. J. Bowick, J. H. Meinke, D. R. Nelson and A. R. Bausch, *Nat. Mater.*, 2005, **4**, 407.
- 56 M. Bowick, A. Cacciuto, D. R. Nelson and A. Travasset, *Phys. Rev. Lett.*, 2002, **89**, 185502.
- 57 P. G. de Gennes and J. Prost, *The Physics of Liquid Crystals, 2nd ed.*, Oxford University Press, 1993.
- 58 G. H. Fredrickson, *The Equilibrium Theory of Inhomogeneous Polymers*, Oxford University Press, 2006.
- 59 D. Marenduzzo and E. Orlandini, *Soft Matter*, 2013, **9**, 1178.

Graphical abstract

Defect Structures and Ordering Behaviours of Diblock Copolymers Self-Assembling on Spherical Substrates

Liangshun Zhang,^{*a} Liquan Wang^a and Jiaping Lin^{*a}



The Landau-Brazovskii theory is employed to explore defect structures and ordering behaviors of block copolymers confined on spherical substrates. The isolated disclinations and scars are formed in the cylindrical phase. The defect structures of hedgehog, spiral and quasi-baseball are produced in the lamellar phase.